Stem Cell Reports
Report
ISSCR
OPEN ACCESS

De novo DNA methyltransferases DNMT3A and DNMT3B are essential for *XIST* silencing for erosion of dosage compensation in pluripotent stem cells

Atsushi Fukuda,[1,2,3,4,5,7,*] Dane Z. Hazelbaker,[2] Nami Motosugi,[3] Jin Hao,[1,2] Francesco Limone,[1,2] Amanda Beccard,[2] Patrizia Mazzucato,[2] Angelica Messana,[2] Chisa Okada,[6] Irune Guerra San Juan,[1,2] Menglu Qian,[1,2] Akihiro Umezawa,[7] Hidenori Akutsu,[7] Lindy E. Barrett,[1,2] and Kevin Eggan[1,2,*]

[1]The Harvard Stem Cell Institute and Department of Stem Cell and Regenerative Biology, Harvard University, Cambridge, MA, USA
[2]Stanley Center for Psychiatric Research, Broad Institute of MIT and Harvard, Cambridge, MA, USA
[3]Department of Molecular Life Science, Division of Basic Medical Science and Molecular Medicine, Tokai University School of Medicine, Isehara, Kanagawa, Japan
[4]The Institute of Medical Science, Tokai University, Kanagawa, Japan
[5]Micro/Nano Technology Center, Tokai University, Hiratsuka, Kanagawa, Japan
[6]Support Center for Medical Research and Education, Tokai University School of Medicine, Isehara, Kanagawa, Japan
[7]Center for Regenerative Medicine, National Center for Child Health and Development, Tokyo, Japan
*Correspondence: fa972942@tsc.u-tokai.ac.jp (A.F.), eggan@mcb.harvard.edu (K.E.)
https://doi.org/10.1016/j.stemcr.2021.07.015

SUMMARY

Human pluripotent stem cells (hPSCs) have proven to be valuable tools for both drug discovery and the development of cell-based therapies. However, the long non-coding RNA *XIST*, which is essential for the establishment and maintenance of X chromosome inactivation, is repressed during culture, thereby causing erosion of dosage compensation in female hPSCs. Here, we report that the *de novo* DNA methyltransferases DNMT3A/3B are necessary for *XIST* repression in female hPSCs. We found that the deletion of both genes, but not the individual genes, inhibited *XIST* silencing, maintained the heterochromatin mark of H3K27me3, and did not cause global overdosage in X-linked genes. Meanwhile, *DNMT3A/3B* deletion after *XIST* repression failed to restore X chromosome inactivation. Our findings revealed that *de novo* DNA methyltransferases are primary factors responsible for initiating erosion of dosage compensation in female hPSCs, and *XIST* silencing is stably maintained in a *de novo* DNA-methylation-independent manner.

INTRODUCTION

During female mammalian development, each cell selects one of the two X chromosomes for inactivation to achieve dosage compensation of gene expression (Augui et al., 2011). A key step in this process, known as X chromosome inactivation (XCI), is established through the expression of the long non-coding X-inactive specific transcript, *XIST* RNA (Augui et al., 2011). Genetic studies in mice have shown that *Xist* is essential for initiation (Marahrens et al., 1997) and normal maintenance of XCI (Csankovszki et al., 2001). However, in both female human induced pluripotent stem cells (iPSCs) and human embryonic stem cells (hESCs) cultured under standard "primed" conditions, the expression of *XIST* is routinely lost (Anguera et al., 2012; Mekhoubad et al., 2012; Patel et al., 2017; Sahakyan et al., 2018). Once *XIST* expression is silenced in a human pluripotent stem cell (hPSC), this state is propagated through subsequent cell divisions and is associated with a loss of the repressive H3K27me3 mark, overlapped with *XIST* RNA (Mekhoubad et al., 2012; Sahakyan et al., 2017; Vallot et al., 2015), as well as widespread changes in DNA CpG methylation (Mekhoubad et al., 2012; Patel et al., 2017; Vallot et al., 2015). Ultimately, these events result in the inappropriate, biallelic expression of X-linked genes and affect the differentiation potential (Mekhoubad et al., 2012; Salomonis et al., 2016; Vallot et al., 2015). These events, which have been dubbed "erosion" of dosage compensation, share many similarities with those occurring after conditional deletion of *Xist* from the mouse inactive X chromosome (Csankovszki et al., 2001; Marahrens et al., 1997).

While conversion to a naive state was suggested to potentially help correct *XIST* repression, the naive cell culture conditions currently known and used have limited ability to restore dosage compensation (Guo et al., 2017; Sahakyan et al., 2017) and may cause chromosomal abnormalities (Liu et al., 2017). Given these observations, it is essential to understand how *XIST* silencing, resulting in erosion of dosage compensation, is induced in hPSCs. An increased mechanistic understanding might in turn allow erosion to be prevented prior to the deployment of female hPSCs in both disease modeling and cell replacement therapies.

RESULTS

Inhibition of DNA methylation reactivates *XIST* during hPSC differentiation

It is well known that the *XIST* locus becomes methylated in male cells, which do not express *XIST*, and remains relatively unmethylated in female cells that do transcribe the RNA (Chapman et al., 2014). The findings from the study suggested that the *XIST*-expressing allele exhibits

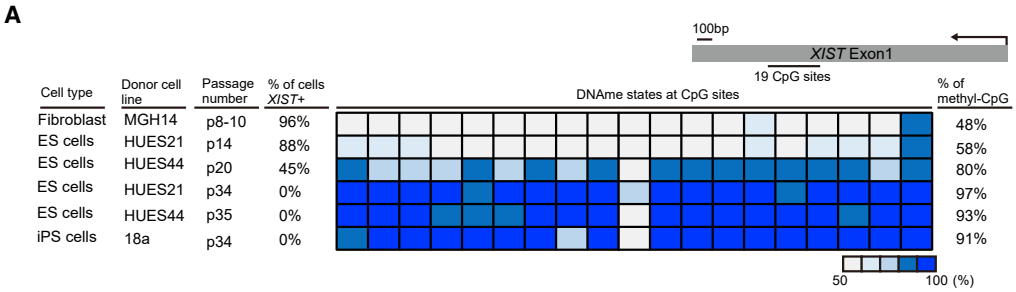

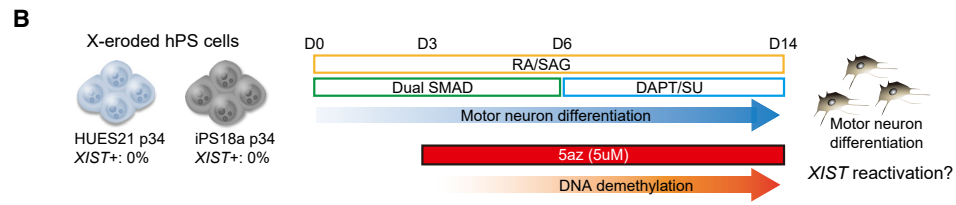

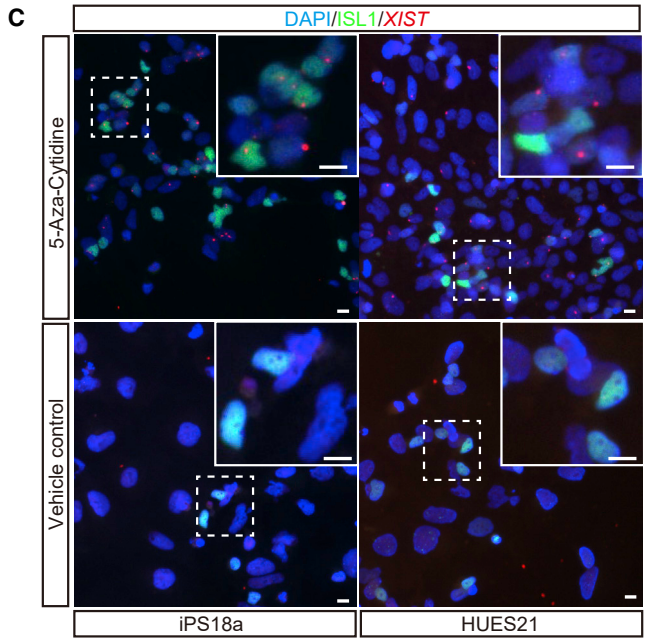

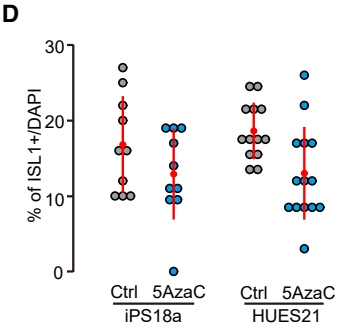

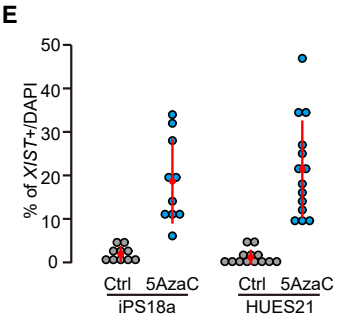

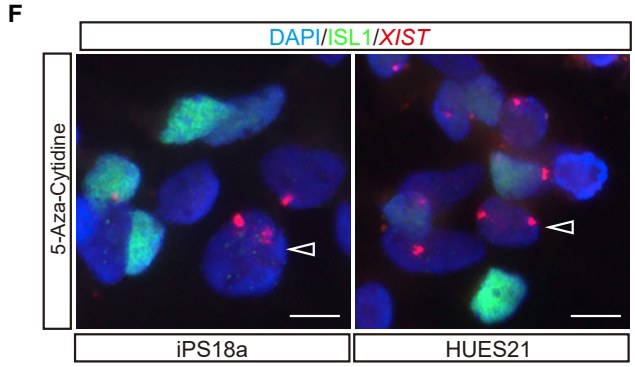

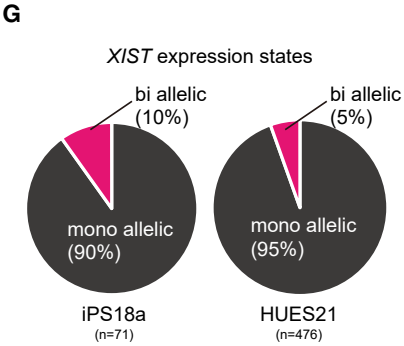

(legend on next page)

approximately 50% DNA methylation, whereas DNA is hypermethylated in cells without *XIST* expression. We previously reported that after erosion of dosage compensation, female hPSCs acquired increased levels of *XIST* methylation, which were similar to those observed in male cells (Mekhoubad et al., 2012). We began our studies by investigating the generality and reproducibility of changes in *XIST* DNA methylation using three different female hPSC lines with distinct passage numbers as well as a somatic cell control. This new analysis of *XIST* DNA methylation by bisulfite sequencing and transcript expression by fluorescence *in situ* hybridization (FISH) confirmed that reduced expression of *XIST* and the onset of erosion did indeed correlate with an increase in *XIST* DNA methylation (Figure 1A).

We next wondered whether these changes in methylation at the *XIST* promoter were merely correlated with *XIST* silencing or instead directly related to its functional repression. To test this idea we attempted to reduce DNA methylation levels in eroded hPSCs by using the DNA methyltransferase inhibitor 5-azacytidine (5azaC) (Christman, 2002). Unfortunately, treatment with 5azaC resulted in rapid hPSC death (Figure S1), consistent with a previous report suggesting that the activity of the maintenance methyltransferase DNMT1 is essential for hPSC self-renewal (Liao et al., 2015). It is also well known that the toxicity of 5azaC is most pronounced in rapidly dividing cells (Szyf, 2011). We therefore next wondered if 5azaC treatment during directed differentiation down the motor neuron lineage would allow cells to survive 5azaC treatment due to their slowing rates of cell division, while still undergoing sufficient DNA replication to enable passive demethylation (Figure 1B). To this end, we initiated a well-established motor neuron differentiation scheme with two eroded cell lines (iPSC 18a and hESC HUES21) and at day 3 of differentiation began administering 5azaC. After 11 additional days of differentiation with 5azaC administration, we quantified the number of ISL1-expressing spinal motor neurons and monitored *XIST* expression by RNA-FISH. As anticipated, the efficiency of motor neuron differentiation decreased in both 5azaC-treated cultures (Figures 1C and 1D), suggesting that 5azaC remained modestly toxic. Despite the negative effect on differentiation, 5azaC treatment led to a substantial and significant induction of *XIST* expression in both eroded cell lines (Figures 1C–1E). Interestingly, we also noted biallelic expression of *XIST* by FISH in a small portion of cells treated with 5azaC (Figures 1F and 1G). Overall, these initial results are consistent with the notion that DNA methylation is required in the differentiating derivatives of hPSCs to maintain silencing of *XIST* on both the active X chromosome and the "eroded" X chromosome following erosion of dosage compensation.

DNMT3A and DNMT3B are essential for *XIST* repression, resulting in erosion of dosage compensation

The *de novo* DNA methyltransferases *DNMT3A* and *DNMT3B* are expressed during pre- and post-preimplantation embryo development, where they mediate the establishment of lineage-specific DNA methylation patterns (Smith et al., 2014). However, we showed that upon explant of the human inner cell mass into culture conditions for hPSC derivation, an immediate and significant increase in genome-wide levels of DNA methylation occurred that was carried over into the resulting hESCs and that is also seen upon human iPSC reprogramming (Meissner, 2010). We wondered whether this increase in DNA methylation found previously might also be related to the accumulation of methylation at *XIST*. If so, we reasoned that elimination of one or both of the *de novo* DNA methyltransferases in hPSCs might prevent *XIST* silencing. To test this idea, we identified a culture of HUES21 that was largely composed of cells still harboring an inactive X (>80%) and then used CRISPR-Cas9 to generate mutant sub-clones harboring homozygous loss-of-function mutations in *DNTM3A* or *DNMT3B* alone, as well as clones with mutations in both of the *de novo* methyltransferases (Figure 2A). We then identified, by DNA sequencing and western blot analysis, appropriate wild type or mutant sub-clones and double mutants cloned that also retained an inactive X chromosome as measured by H3K27me3 staining (Figures 2A, 2B, S2A, and S2B).

Using the resulting mutant, double mutant, and control sub-clones, we performed continuous cell culture over 18 days and monitored the erosion of dosage compensation by measuring the expression of *XIST* and the X-active specific transcript (*XACT*), a marker of erosion (Vallot et al.,

Figure 1. DNA methylation suppresses *XIST* expression after erosion of dosage compensation

(A) Bisulfite sequence analysis at *XIST* in hPSCs and a somatic cell line. The percentage of *XIST* expression state was determined by RNA-FISH experiments.

(B) Experimental scheme for motor neuron differentiation with 5azaC.

(C) Immunofluorescence staining (ISL1) combined with *XIST* RNA-FISH at day 14. The scale bar represents 10 μm.

(D and E) Quantification of ISL1- (D) and *XIST*-positive (E) cells relative to DAPI in iPS18a and HUES21 p34. Each dot indicates the percentage of ISL- or *XIST*-positive cells in the observed area in two independent experiments. In each group, >424 cells were analyzed.

(F and G) Immunofluorescence staining (F) and quantification (G) of cells with *XIST* mono- and biallelic expression. The arrowheads indicate cells with biallelic *XIST* expression. The scale bar represents 10 μm. n means the number of cells analyzed.

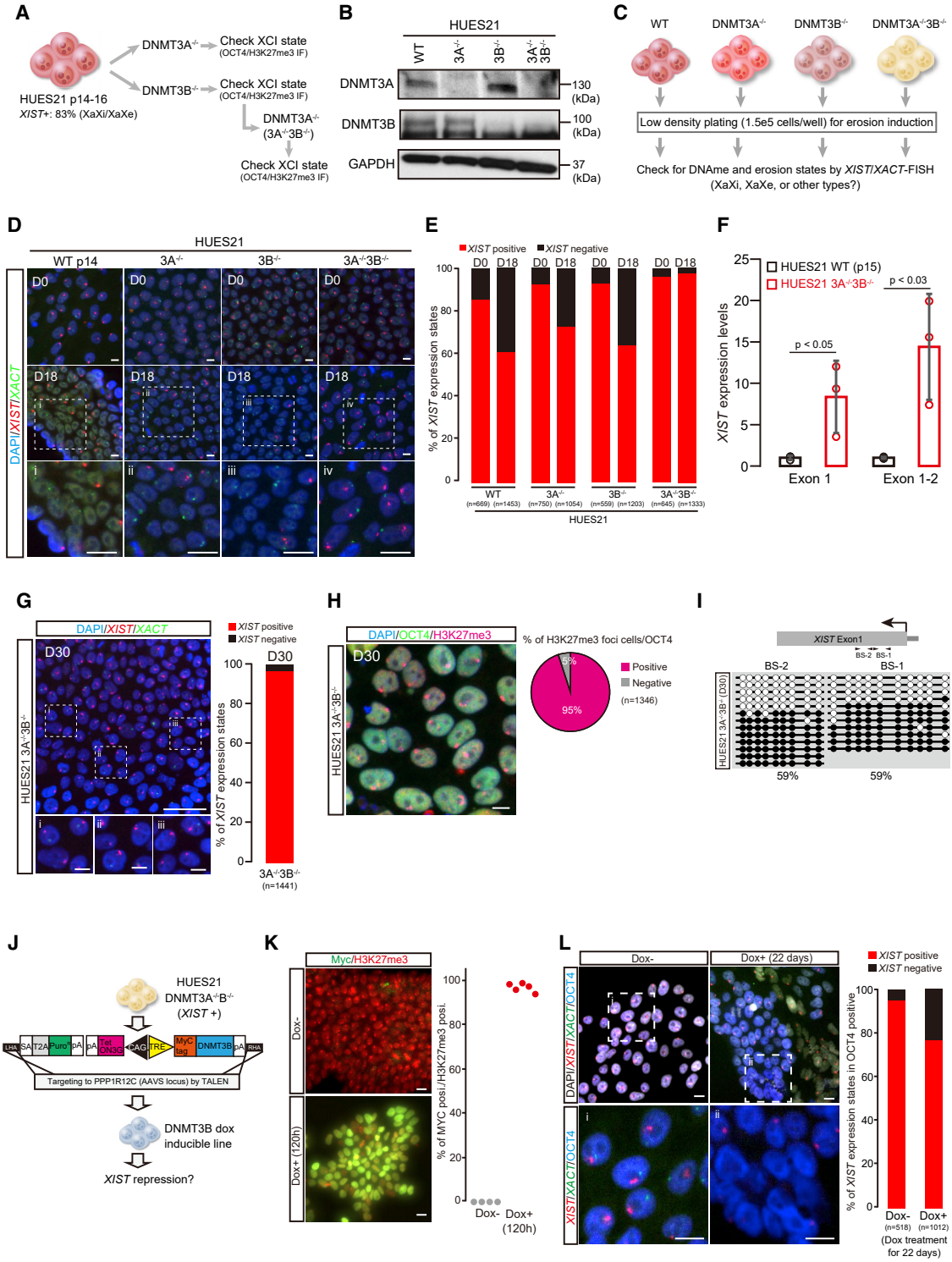

Figure 2. Eliminating DNMT3A/3B prevents erosion of dosage compensation

(A) Experimental scheme for generation of single DNMT3A, single DNMT3B, and double knockout lines. All the knockout lines were produced by the CRISPR-Cas9 system. The *XIST*-positive line HUES21 p14-16 was used as the parental line. After genotyping, OCT4/H3K27me3 immunofluorescence was used to determine XCI state in each clone. See also Figure S2B.

(B) Western blotting for DNMT3A and DNMT3B. GAPDH was used as the loading control. In DNMT3B, the upper band is the targeted size.

(legend continued on next page)

2015), by RNA-FISH (Figures 2C–2E). The quantification of *XIST* and *XACT* transcripts revealed that over the same growth period, a significantly large number of wild-type, single 3A$^{-/-}$, and single 3B$^{-/-}$ mutant cells had lost *XIST* expression and begun to express *XACT* from the eroded X chromosome (Figures 2C–2E). In striking contrast, >95% of *DNMT3A/B* compound mutant cells retained expression of *XIST* on the inactive X chromosome and *XACT* on the one presumptive active X (Figures 2C–2E). Protection of *XIST* expression levels in DNMT3A$^{-/-}$3B$^{-/-}$ compound mutant cells after sustained culture was also readily detected by *XIST* qRT-PCR compared with the wild-type HUES21 clone that had undergone erosion of dosage compensation while being grown in parallel (Figure 2F).

To test the durability of the protection from erosion of dosage compensation conferred by eliminating DNMT3A and DNMT3B, we continued to culture the double-mutant cells for a total of 30 days and found that the inactive X chromosome was still properly maintained in >95% of cells as measured by *XIST* RNA-FISH and immunostaining for H3K27me3 (Figures 2G and 2H). We also determined that a small proportion of cells exhibited no *XIST* expression; however, this was likely the result of experimental detection efficiency, since it was also observed in human primary fibroblasts (Figure 1A). DNA methylation at the *XIST* locus revealed that DNTM3A$^{-/-}$;DNMT3B$^{-/-}$ mutant cells maintained methylation levels appropriately on 50% of sequences analyzed (Figure 2I), similar to the status of DNA methylation in the non-eroded wild type (Figure 1A).

To confirm that the protection from erosion of dosage compensation observed in double *DNMT3A/3B* mutants was due to the loss of methyltransferase activity, we rescued *DNMT3B* expression by a doxycycline (dox)-inducible system targeted to the AAVS locus in double *DNMT3A/3B* mutants of the HUES21 line (Figures 2J–2L). In the absence of dox, these cells retained a clear inactive X as measured by *XIST* expression (Figure 2L). However, upon dox addition and induction of DNMT3B expression, the cells rapidly began to lose *XIST* expression (Figures 2K and 2L).

We further examined whether deletion of *DNMT3A/3B* can prevent erosion of dosage compensation in different female hPSC lines. Using the ADSC-iPS line derived from adipose stem cells with XCI maintained in most early passage cells, while *XACT* biallelic expression was observed at high passage (Figures S2C and S2D), we generated homogeneous DNMT3A$^{-/-}$3B$^{-/-}$ mutant cells using the population with a high proportion of XCI-positive cells (Figures S2C–S2F). Thirty days after low-density plating to induce erosion, we examined XCI state by immunostaining for H3K27me3 and OCT4 (Figure S2G). The DNMT3A$^{-/-}$3B$^{-/-}$ ADSC-iPS line maintained H3K27me3 foci in >95% of OCT4-positive cells, while the wild type exhibited a lower population with H3K27me3 foci (Figure S2H). Taken together, our findings clearly demonstrate that elimination of both *de novo* DNA methyltransferases prevents *XIST* silencing, leading to the erosion of dosage compensation.

Deletion of DNMT3A/3B does not cause global overdosage of X-linked genes, but the effect on transcriptome status depends on genetic background

Since DNA methylation status and erosion of dosage compensation affects transcriptomes (Mekhoubad et al.,

(C) Experimental scheme for erosion induction and assessment of erosion state.
(D) *XIST/XACT* RNA-FISH assay. At day 18 after low-density plating, each line was analyzed. The scale bar indicates 10 μm.
(E) Quantification of *XIST/XACT* expression state by RNA-FISH. n, number of cells analyzed. A detailed classification of the results is shown in Figure S4A.
(F) qPCR analysis of *XIST* expression level in wild-type (WT) HUES21 p15 and DNMT3A$^{-/-}$3B$^{-/-}$ lines. A t test was used for statistical calculation.
(G) *XIST/XACT* expression state by RNA-FISH in DNMT3A$^{-/-}$3B$^{-/-}$ at day 30 after low-density plating. Note that the DNMT3A$^{-/-}$3B$^{-/-}$ line was cultured for several months for gene editing before the low-density plating experiments. The scale bar represents 50 μm. The scale bars for images (i)–(iii) represent 10 μm. n, number of cells analyzed. The categories of expression state are the same as in (D). Two independent experiments were conducted.
(H) H3K27me3/OCT4 immunofluorescence analysis in DNMT3A$^{-/-}$3B$^{-/-}$ at day 30. The scale bar represents 10 μm. The quantification results of H3K27me3 foci in OCT4-positive cells are shown as a pie chart. n, number of analyzed cells. Two independent experiments were conducted.
(I) DNA methylation (DNAme) state at *XIST* promoter regions in DNMT3A$^{-/-}$3B$^{-/-}$ at day 30. BS-1 and BS-2 indicate CpG regions examined by bisulfite sequence.
(J) Experimental scheme of DNMT3B doxycycline (dox)-inducible system in the HUES21 DNMT3A$^{-/-}$3B$^{-/-}$ line from the AAVS locus.
(K) Immunofluorescence analysis of Myc-tag and H3K27me3 at 120 h after dox treatment. Each dot shows the percentage of MYC-positive cells with H3K27me3 signal in observed areas. Two independent experiments were conducted.
(L) Immunofluorescence combined with *XIST/XACT* RNA-FISH analysis in *DNMT3B* inducible line after long-term dox treatment. The dox treatment was conducted for 22 days. OCT4 was used as the undifferentiated hPSC and *XIST* population was determined by only OCT4-positive cells. Two independent experiments were conducted. A detailed classification of the results is shown in Figure S4B. The scale bars represent 10 μm. n, number of cells analyzed.

2012), we examined the impact of double *DNMT3A/3B* mutants on transcriptional profiles in female hPSCs. We performed RNA sequencing on non-eroded wild type (*XIST*$^{+}$ population), eroded wild type (*XIST*$^{-}$ population), and DNMT3A$^{-/-}$3B$^{-/-}$ in the ADSC-iPS and HUES21 lines (Figure 3A). We first ascertained whether X chromosome upregulation occurs by deletion of *de novo* DNA methyltransferases. Based on previous studies (Fukuda et al., 2015; Sangrithi et al., 2017), we employed a computational approach to evaluate the expression ratio between X-linked genes and autosomal genes (X:A) at the chromosome scale using the median expression levels of transcripts per million (TPM), which enables the comparison of expression levels among genes in the same sample. Bootstrap analysis showed that the ratios of the eroded ADSC-iPS and HUES21 cell lines were higher than those of the non-eroded wild-type cell lines (Figure 3B), consistent with previous results (Patel *et al.*, 2017). We found that the ratios of the DNMT3A$^{-/-}$3B$^{-/-}$ cell lines were lower than those of the eroded wild type (Figure 3B), suggesting that, unlike eroded lines, X-linked genes are not overexpressed. However, we did not exclude the possibility that the lower ratios of X:A in the DNMT3A$^{-/-}$3B$^{-/-}$ cell lines resulted from the upregulation of autosomal genes. To test this hypothesis, we checked the global expression status of autosomal and X-linked genes. We did not observe significant upregulation of X-linked genes compared with autosomal genes in the DNMT3A$^{-/-}$3B$^{-/-}$ cell lines (Figure S2I); however, it markedly reduced the expression levels of the mutant line in the HUES21 background (Figure S2I). Thus, these results indicated that, unlike in eroded lines, deletion of DNMT3A/3B did not cause global upregulation of X-linked genes.

Next, we explored whether global gene expression status in the mutant cell lines was similar to that in the non-eroded wild-type cell lines. To address the transcriptional similarity, we conducted hierarchical clustering analysis using trimmed mean of M (TMM) values suitable for direct comparisons between different samples (Robinson and Oshlack, 2010). Interestingly, analysis using X-linked genes indicated clear segregation based on XCI state in ADSC-iPS lines rather than genotype (Figure 3C). In contrast, the expression state of X-linked genes in the HUES21 line was markedly affected by *DNMT3A/3B* mutations (Figure 3C), consistent with a previous study using male hPSCs (Liao et al., 2015). Similarly, hierarchical clustering analysis using all transcripts, including autosomal genes, also separated ADSC-iPS by XCI state and HUES21 by genotype (Figure 3D). We also confirmed the same results when using the TPM normalization method (not shown). Consistent with the clustering results, the mean absolute deviation in the expression ratio of the eroded wild-type cell lines compared with the non-eroded wild-type cell lines was greater than that of DNMT3A$^{-/-}$3B$^{-/-}$ cells in the ADSC-iPS background, while it was greater in DNMT3A$^{-/-}$3B$^{-/-}$ cells in the HUES21 background (Figure 3E).

Taken together, deletion of DNMT3A/3B in non-eroded cell lines does not cause global overdosage of X-linked genes in DNMT3A$^{-/-}$3B$^{-/-}$ cells, but the similarity of global transcriptional status of DNMT3A$^{-/-}$3B$^{-/-}$ cell to non-eroded cell differs in the cell lines.

Loss of DNMT3A and DNMT3B cannot reactivate *XIST* after erosion of dosage compensation

Once established by *de novo* methylation, patterns of DNA methylation are generally maintained by *DNMT1* (Law and Jacobsen, 2010). However, we considered the possibility that eliminating one or both *de novo* DNA methyltransferases after erosion of dosage compensation might still rescue X inactivation (Figure 4A). To address this possibility, we generated wild-type, DNMT3A$^{-/-}$, DNMT3B$^{-/-}$, and DNMT3A$^{-/-}$3B$^{-/-}$ compound mutant sub-clones from a later passage of HUES21 (p34), which had undergone dosage compensation and completely lacked *XIST* expression (Figure 4A). After genotyping and confirming the mutations by western blot analysis (Figures 4B and S2J), we performed prolonged cell culture and then examined the X chromosome (Figure 4C). Unfortunately, we did not find evidence for restoration of dosage compensation by measurement of *XIST*/*XACT* RNA-FISH (Figures 4D and 4E), immunostaining for H3K27me3 (Figure S2K), or *XIST* DNA methylation (Figure 4F). Thus, it appears that once ectopic DNA methylation is established by DNMT3A or DNMT3B and *XIST* expression is silenced, it is faithfully maintained, likely by *DNMT1*, even in the absence of the *de novo* methyltransferases (Figure 4G).

XIST reactivation by the CRISPR activation system cannot reinitiate heterochromatinization

Because ectopic *XIST* expression can reinitiate heterochromatinization *in cis* (Jiang et al., 2013), we considered whether endogenous *XIST* activation by the CRISPR activation (CRISPRa) system would be a useful approach to rescue dosage compensation in eroded female hPSC lines. Using the dCas9:VPR:T2A:GFP fusion gene with the dox-inducible system at the AAVS safe harbor locus (Hazelbaker et al., 2020), we generated *XIST*-inducible lines from the iPS18a line that showed complete *XIST* loss by RNA-FISH (Figures S3A and 1A). We used U6 promoter-driven expression of guide RNAs (gRNAs) that were specific to the *XIST* promoter region from an additional PiggyBac transgene, which also encoded a constitutive red fluorescent reporter gene (Figure S3B). We also assessed whether there was a potential bias in the genomic sequence for gRNA binding, revealing the absence of single-nucleotide variance at the

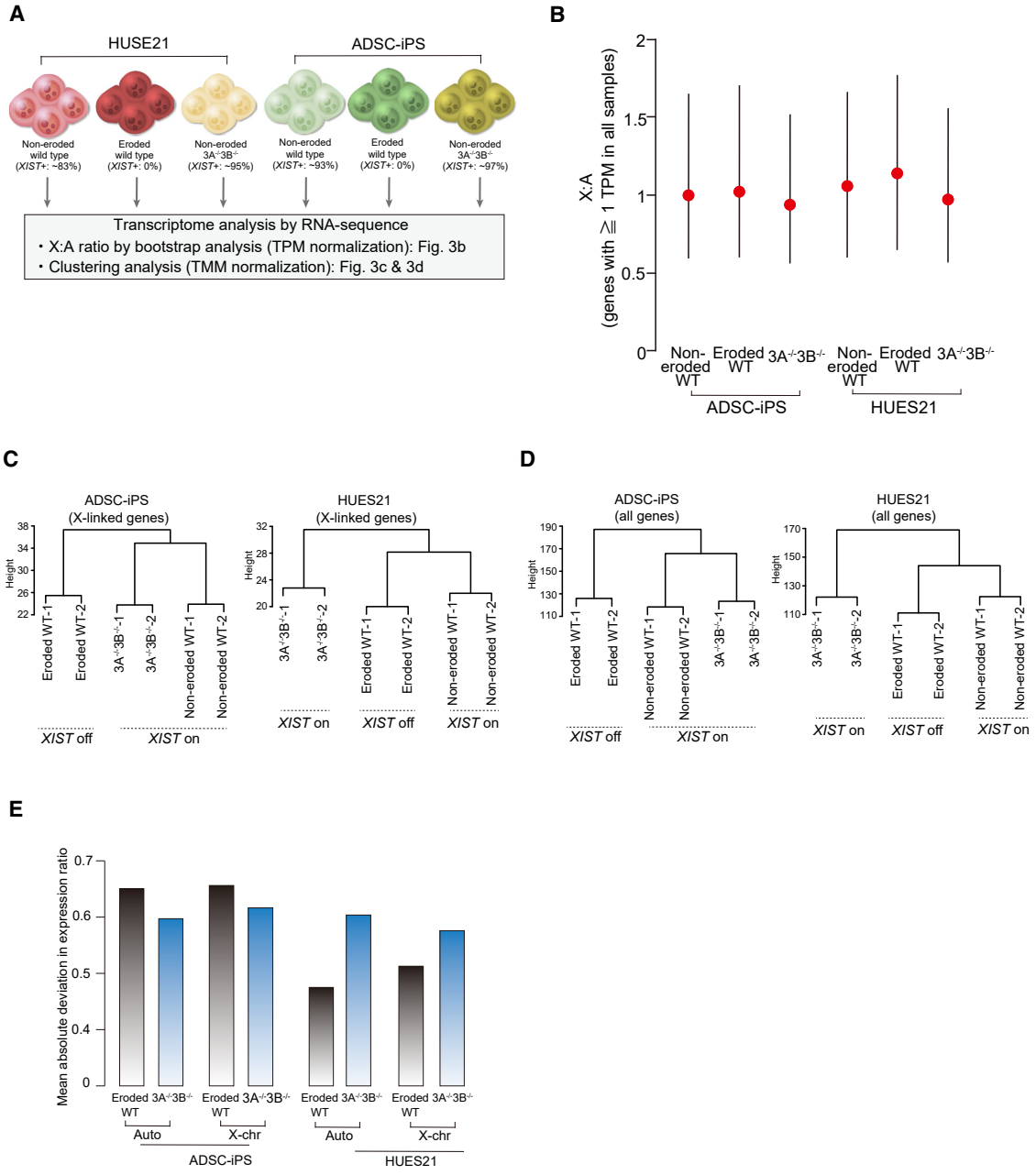

Figure 3. Influence of *DNMT3A* and *DNMT3B* double mutations on transcriptional status

(A) Experimental scheme for RNA-sequence analysis. Non-eroded (wild type), eroded (wild type), and DNMT3A$^{-/-}$3B$^{-/-}$ in the HUES21 and ADSC-iPS lines were used for the assay. In each line, two replicates were analyzed.

(B) Bootstrapped X:A ratios in each cell line. Genes with $\geq$1 TPM in all cell lines were used for the assay. X:A ratios with 95% confidence intervals are shown and the mean ratio is indicated by a red circle.

(C and D) Hierarchical clustering analysis using X-linked genes (C) and all genes (D). TMM normalization was employed and genes with >1 TMM in each cell line were used.

(E) Bar plot illustrating the mean absolute deviation in expression ratios of eroded or DNMT3A$^{-/-}$3B$^{-/-}$ cell lines compared with non-eroded wild-type cell lines. The genes used in the hierarchical clustering analysis were used for the calculation.

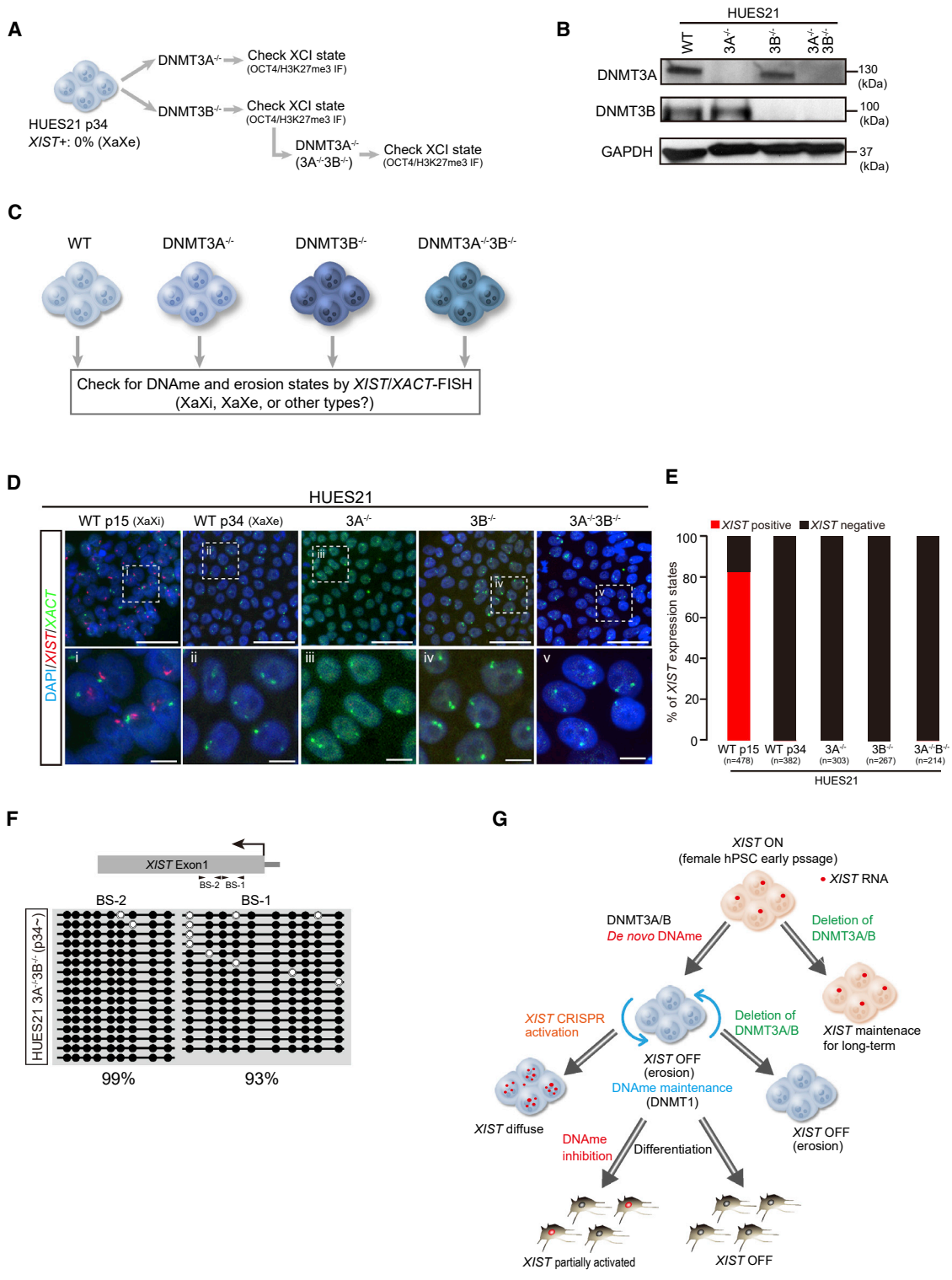

Figure 4. DNMT3A/3B deletion does not rescue *XIST* expression after dosage compensation erosion

(A) Experimental scheme for the generation of DNMT3A/3B knockout lines. HUES21 p34 (*XIST*$^{+}$ 0%) was used as the parental line.

(B) Western blotting for DNMT3A and DNMT3B. GAPDH was used as the loading control.

(C) Experimental scheme to examine the effect of deletion of *de novo* DNA methyltransferases on eroded lines.

(D) *XIST/XACT* RNA-FISH assay. Scale bars represent 10 μm.

(legend continued on next page)

three gRNA sites (Figure S3C). To validate this system, we performed chromatin immunoprecipitation with antibodies specific to the Cas9 protein, followed by quantitative PCR (qPCR). Upon dox induction of Cas9:VPR expression, we found it localized to two *XIST* promoter regions adjacent to the sites of gRNA complementarity, but not to a region farther 5′ of the promoter nor to a region downstream in exon 1 (Figure S3D).

We next examined *XIST* expression by qPCR at 48 and 96 h post-dox induction in two independent clones (iPS18a *XIST*i-1 and iPS18a *XIST*i-2). At 48 h after dox administration, we found an increase in *XIST* expression (>89-fold in iPS18a*XIST*i-1 and >9-fold in iPS18a*XIST*i-2), which continued to increase to significance at 96 h compared with the no-dox control (Figure S3E). These results demonstrated that the dCas9-VPR system could induce endogenous *XIST* expression.

We performed *XIST* RNA-FISH to ask whether the *XIST* transcripts induced by CRISPRa could localize to either the eroded or the active X chromosome and reinitiate heterochromatization. However, upon dox induction of CRISPRa, the *XIST* signal became clearly detected by FISH in 20% of 18a cells from each of the two independent clones (Figures S3F–S3H). We noted that this failure to detect *XIST* in the majority of cells was not due to transgene silencing, as both GFP and RFP were widely expressed after dox administration (Figure S3B). We further noted that, in the CRISPRa cells in which we did observe *XIST* signal, *XIST* did not localize to a clear single focus of expression, as it did in the control cell line with an inactive X (HUES21). Instead, after CRISPRa, *XIST* was expressed in a diffuse pattern throughout the nucleus (Figure S3H). Moreover, at 96 h of dox treatment, immunostaining with antibodies specific for H3K27me3 failed to detect signs of reinitiation of heterochromatin formation on the X (Figure S3I). To rule out the possibility that CRISPRa had simply failed to induce sufficient *XIST* expression to reinactivate the eroded X chromosome, we transfected additional dCas9-VPR and gRNA transgenes into the iPS18a*XIST*i-1 cell line (Figure S3J). After 48 h of dox induction in the cells, qPCR analysis revealed that the *XIST* expression levels were significantly elevated and were >60% of those in HUES21 cells (p13) (Figure S3K). Despite this further increase in expression, RNA-FISH still revealed an unusual localization for *XIST*, with many cells showing strong punctate signals throughout the nucleus, which again failed to colocalize with H3K27me3 (Figures S3L and S3M). Thus, while we had been successful in using CRISPRa to reactivate *XIST* expression in stem cells that had undergone X chromosome erosion, we found it could not reinitiate dosage compensation.

DISCUSSION

Erosion of dosage compensation is one of the single largest sources of epigenetic as well as functional variation in the behavior of female pluripotent stem cells and their differentiated derivatives (Mekhoubad et al., 2012). It would therefore be beneficial for translational stem cell applications if a path could be found for preventing this process from occurring. Given our findings that *DNMT3A/3B* initiate erosion of dosage compensation and the known importance of these enzymes for stem cell differentiation (Ziller et al., 2018), transient or reversible repression of these enzymes during hPSC culture might be useful.

Another interesting observation in our study was the diffuse *XIST* RNA induced by the CRISPR activation system. The aberrant transcribed RNA behavior suggested that *XIST* RNA from a silenced allele(s) might not interact with factors required for *cis* action. Among the proteins that interact with *XIST* RNA, YY1, SAF-A, and CIZ1 are involved in *XIST*/*Xist* RNA diffusion (Loda and Heard, 2019). Since the effect of *XIST* RNA diffusion depends on cell lines (Kolpa et al., 2016), YY1 and CIZ1 are thought to be candidates responsible for the failure of XIST RNA *cis* action by the CRISPR activation system. Given that both YY1 and CIZ1 are highly expressed in female eroded hPSC lines (RNA-sequencing data not shown), protein binding to the *XIST* genomic region might be prevented in the eroded cell line. Although CIZ1 binding to the *Xist* genome depends on repeat E in mice (Loda and Heard, 2019), it remains unknown whether repeat E mutations or epigenetic modifications occur during erosion. In contrast, YY1 binds to *XIST* promoter regions in a DNA-methylation-dependent manner (Makhlouf et al., 2014). Considering our findings that *XIST* expression depends on DNA methylation, unbinding of YY1 to the promoter regions might be one of the causes of the diffusion of *XIST* RNA by the CRISPR activation system.

(E) Quantification of *XIST*/*XACT* expression state. n means the number of cells analyzed. A detailed classification of the results is shown in Figure S4C. Two independent experiments were conducted.

(F) DNA methylation state at *XIST* promoter regions in DNMT3A$^{-/-}$3B$^{-/-}$ generated using eroded HUES21 p34.

(G) Model of *XIST* silencing to initiate erosion in female hPSCs. *De novo* DNA methyltransferases methylate *XIST* to silence its expression. Once *XIST* is silenced, deletion of DNMT3A/3B cannot reactivate *XIST* and the states are stably maintained, likely by DNMT1. During differentiation, demethylation can partially reactivate *XIST*, but forced activation of endogenous *XIST* in eroded hPSCs generates diffused transcripts that cannot act to cause heterochromatization.

Given that erosion of dosage compensation occurs in female hPSC lines, it might be tempting to prioritize the use of male cells for the development of allogenic or other therapies. However, we argue that if women are to optimally and equally benefit from future hPSC therapies, especially autologous therapies, it must remain a priority to develop methods to eliminate erosion of dosage compensation.

EXPERIMENTAL PROCEDURES

hPSC culture

HUES21 and iPS18a lines were cultured in mTeSer medium (STEMCELL Technologies) without feeder cells or on irradiated CF1 mouse embryonic fibroblasts (Thermo Fisher Scientific) with standard hPSC medium. The detailed description is provided in the supplemental experimental procedures.

Motor neuron differentiation

Motor neuron differentiation was performed based on a previous report (Klim et al., 2019). The detailed description is provided in the supplemental experimental procedures.

Generation of single DNMT3A, single DNMT3B, and double knockout lines

For the generation of DNMT3A/3B knockout lines, we used the CRISPR-Cas9 system with the gRNAs previously validated (Liao et al., 2015). The detailed description is provided in the supplemental experimental procedures.

RNA-FISH

RNA-FISH experiments were performed based on a previous report (Fukuda et al., 2016). The detailed description of the method and classification of the results are provided in the supplemental experimental procedures and Figures S4A–S4C, respectively.

Data and code availability

RNA-sequencing data from this study have been deposited in the GEO database (GSE160454).

SUPPLEMENTAL INFORMATION

Supplemental information can be found online at https://doi.org/10.1016/j.stemcr.2021.07.015.

AUTHOR CONTRIBUTIONS

A.F. and K.E. conceived and designed the study. A.F. generated all of gene-manipulated cell lines, developed the construct for the 18a*XIST*i lines, and conducted most of the experiments and analysis. D.H., A.B., P.M., A.M., and L.B. designed and developed constructs and tools for generation of CRISPRa 18a*XIST*i lines and analyzed the data. N.M. and C.O. analyzed data and helped in the generation of gene-manipulated cell lines, FISH, and western blotting experiments. H.A. and A.U. generated the ADSC-iPS line. J.H. helped culture cells and in western blotting experiments. F.L. helped culture cells. I.G. helped with differentiation experiments. M.Q. helped with western blotting and immunofluorescence staining experiments. A.F. and K.E. wrote the manuscript with input from all coauthors.

CONFLICT OF INTERESTS

K.E. is a cofounder of Q-State Biosciences, Quralis, and Enclear Therapies, and is group vice president at BioMarin Pharmaceutical.

ACKNOWLEDGMENTS

We would like to thank G. Pintacuda, J. Klim, and H. Kobayashi for their helpful discussion and S. Kikugawa for assistance in bioinformatic analysis. We also thank M. Charlton for her assistance in many aspects of this study. A.F. was supported by JSPS Postdoctoral Fellowships for Research Abroad and is currently supported by the JSPS Leading Initiative for Excellent Young Researchers (LEADER) and by AMED under grant JP21bm0704038. K.E. was supported by grants from the NIGMS P01 (grant GM099117) and the Stanley Center for Psychiatric Research at the Broad Institute.

Received: May 11, 2021
Revised: July 21, 2021
Accepted: July 21, 2021
Published: August 19, 2021

REFERENCES

Anguera, M.C., Sadreyev, R., Zhang, Z., Szanto, A., Payer, B., Sheridan, S.D., Kwok, S., Haggarty, S.J., Sur, M., Alvarez, J., et al. (2012). Molecular signatures of human induced pluripotent stem cells highlight sex differences and cancer genes. Cell Stem Cell *11*, 75–90. https://doi.org/10.1016/j.stem.2012.03.008.

Augui, S., Nora, E.P., and Heard, E. (2011). Regulation of X-chromosome inactivation by the X-inactivation centre. Nat. Rev. Genet. *12*, 429–442. https://doi.org/10.1038/nrg2987.

Chapman, A.G., Cotton, A.M., Kelsey, A.D., and Brown, C.J. (2014). Differentially methylated CpG island within human XIST mediates alternative P2 transcription and YY1 binding. BMC Genet. *15*, 89. https://doi.org/10.1186/s12863-014-0089-4.

Christman, J.K. (2002). 5-Azacytidine and 5-aza-2′-deoxycytidine as inhibitors of DNA methylation: mechanistic studies and their implications for cancer therapy. Oncogene *21*, 5483–5495. https://doi.org/10.1038/sj.onc.1205699.

Csankovszki, G., Nagy, A., and Jaenisch, R. (2001). Synergism of Xist RNA, DNA methylation, and histone hypoacetylation in maintaining X chromosome inactivation. J. Cell Biol. *153*, 773–784. https://doi.org/10.1083/jcb.153.4.773.

Fukuda, A., Mitani, A., Miyashita, T., Sado, T., Umezawa, A., and Akutsu, H. (2016). Maintenance of xist imprinting depends on chromatin condensation state and Rnf12 dosage in mice. PLoS Genet. *12*, e1006375. https://doi.org/10.1371/journal.pgen.1006375.

Fukuda, A., Tanino, M., Matoba, R., Umezawa, A., and Akutsu, H. (2015). Imbalance between the expression dosages of X-chromosome and autosomal genes in mammalian oocytes. Sci. Rep. *5*, 14101. https://doi.org/10.1038/srep14101.

Guo, G., von Meyenn, F., Rostovskaya, M., Clarke, J., Dietmann, S., Baker, D., Sahakyan, A., Myers, S., Bertone, P., Reik, W., et al. (2017). Epigenetic resetting of human pluripotency. Development *144*, 2748–2763. https://doi.org/10.1242/dev.146811.

Hazelbaker, D.Z., Beccard, A., Angelini, G., Mazzucato, P., Messana, A., Lam, D., Eggan, K., and Barrett, L.E. (2020). A multiplexed gRNA piggyBac transposon system facilitates efficient induction of CRISPRi and CRISPRa in human pluripotent stem cells. Sci. Rep. *10*, 635. https://doi.org/10.1038/s41598-020-57500-1.

Jiang, J., Jing, Y., Cost, G.J., Chiang, J.C., Kolpa, H.J., Cotton, A.M., Carone, D.M., Carone, B.R., Shivak, D.A., Guschin, D.Y., et al. (2013). Translating dosage compensation to trisomy 21. Nature *500*, 296–300. https://doi.org/10.1038/nature12394.

Klim, J.R., Williams, L.A., Limone, F., Guerra San Juan, I., Davis-Dusenbery, B.N., Mordes, D.A., Burberry, A., Steinbaugh, M.J., Gamage, K.K., Kirchner, R., et al. (2019). ALS-implicated protein TDP-43 sustains levels of STMN2, a mediator of motor neuron growth and repair. Nat. Neurosci. *22*, 167–179. https://doi.org/10.1038/s41593-018-0300-4.

Kolpa, H.J., Fackelmayer, F.O., and Lawrence, J.B. (2016). SAF-A requirement in anchoring XIST RNA to chromatin varies in transformed and primary cells. Dev. Cell *39*, 9–10. https://doi.org/10.1016/j.devcel.2016.09.021.

Law, J.A., and Jacobsen, S.E. (2010). Establishing, maintaining and modifying DNA methylation patterns in plants and animals. Nat. Rev. Genet. *11*, 204–220. https://doi.org/10.1038/nrg2719.

Liao, J., Karnik, R., Gu, H., Ziller, M.J., Clement, K., Tsankov, A.M., Akopian, V., Gifford, C.A., Donaghey, J., Galonska, C., et al. (2015). Targeted disruption of DNMT1, DNMT3A and DNMT3B in human embryonic stem cells. Nat. Genet. *47*, 469–478. https://doi.org/10.1038/ng.3258.

Liu, X., Nefzger, C.M., Rossello, F.J., Chen, J., Knaupp, A.S., Firas, J., Ford, E., Pflueger, J., Paynter, J.M., Chy, H.S., et al. (2017). Comprehensive characterization of distinct states of human naive pluripotency generated by reprogramming. Nat. Methods *14*, 1055–1062. https://doi.org/10.1038/nmeth.4436.

Loda, A., and Heard, E. (2019). Xist RNA in action: past, present, and future. PLoS Genet. *15*, e1008333. https://doi.org/10.1371/journal.pgen.1008333.

Makhlouf, M., Ouimette, J.F., Oldfield, A., Navarro, P., Neuillet, D., and Rougeulle, C. (2014). A prominent and conserved role for YY1 in Xist transcriptional activation. Nat. Commun. *5*, 4878. https://doi.org/10.1038/ncomms5878.

Marahrens, Y., Panning, B., Dausman, J., Strauss, W., and Jaenisch, R. (1997). Xist-deficient mice are defective in dosage compensation but not spermatogenesis. Genes Dev. *11*, 156–166.

Meissner, A. (2010). Epigenetic modifications in pluripotent and differentiated cells. Nat. Biotechnol. *28*, 1079–1088. https://doi.org/10.1038/nbt.1684.

Mekhoubad, S., Bock, C., de Boer, A.S., Kiskinis, E., Meissner, A., and Eggan, K. (2012). Erosion of dosage compensation impacts human iPSC disease modeling. Cell Stem Cell *10*, 595–609. https://doi.org/10.1016/j.stem.2012.02.014.

Patel, S., Bonora, G., Sahakyan, A., Kim, R., Chronis, C., Langerman, J., Fitz-Gibbon, S., Rubbi, L., Skelton, R.J.P., Ardehali, R., et al. (2017). Human embryonic stem cells do not change their X inactivation status during differentiation. Cell Rep. *18*, 54–67. https://doi.org/10.1016/j.celrep.2016.11.054.

Robinson, M.D., and Oshlack, A. (2010). A scaling normalization method for differential expression analysis of RNA-seq data. Genome Biol. *11*, R25. https://doi.org/10.1186/gb-2010-11-3-r25.

Sahakyan, A., Kim, R., Chronis, C., Sabri, S., Bonora, G., Theunissen, T.W., Kuoy, E., Langerman, J., Clark, A.T., Jaenisch, R., and Plath, K. (2017). Human naive pluripotent stem cells Model X chromosome dampening and X inactivation. Cell Stem Cell *20*, 87–101. https://doi.org/10.1016/j.stem.2016.10.006.

Sahakyan, A., Yang, Y., and Plath, K. (2018). The role of xist in X-chromosome dosage compensation. Trends Cell Biol. *28*, 999–1013. https://doi.org/10.1016/j.tcb.2018.05.005.

Salomonis, N., Dexheimer, P.J., Omberg, L., Schroll, R., Bush, S., Huo, J., Schriml, L., Ho Sui, S., Keddache, M., Mayhew, C., et al. (2016). Integrated genomic analysis of diverse induced pluripotent stem cells from the progenitor cell biology consortium. Stem Cell Rep. *7*, 110–125. https://doi.org/10.1016/j.stemcr.2016.05.006.

Sangrithi, M.N., Royo, H., Mahadevaiah, S.K., Ojarikre, O., Bhaw, L., Sesay, A., Peters, A.H., Stadler, M., and Turner, J.M. (2017). Non-canonical and sexually dimorphic X dosage compensation states in the mouse and human germline. Dev. Cell *40*, 289–301 e283. https://doi.org/10.1016/j.devcel.2016.12.023.

Smith, Z.D., Chan, M.M., Humm, K.C., Karnik, R., Mekhoubad, S., Regev, A., Eggan, K., and Meissner, A. (2014). DNA methylation dynamics of the human preimplantation embryo. Nature *511*, 611–615. https://doi.org/10.1038/nature13581.

Szyf, M. (2011). The implications of DNA methylation for toxicology: toward toxicomethylomics, the toxicology of DNA methylation. Toxicol. Sci. *120*, 235–255. https://doi.org/10.1093/toxsci/kfr024.

Vallot, C., Ouimette, J.F., Makhlouf, M., Feraud, O., Pontis, J., Come, J., Martinat, C., Bennaceur-Griscelli, A., Lalande, M., and Rougeulle, C. (2015). Erosion of X Chromosome inactivation in human pluripotent cells initiates with XACT coating and depends on a specific heterochromatin landscape. Cell Stem Cell *16*, 533–546. https://doi.org/10.1016/j.stem.2015.03.016.

Ziller, M.J., Ortega, J.A., Quinlan, K.A., Santos, D.P., Gu, H., Martin, E.J., Galonska, C., Pop, R., Maidl, S., Di Pardo, A., et al. (2018). Dissecting the functional consequences of de novo DNA methylation dynamics in human motor neuron differentiation and physiology. Cell Stem Cell *22*, 559–574 e559. https://doi.org/10.1016/j.stem.2018.02.012.